Eur. Phys. J. C 22, 341–349 (2001)
Digital Object Identifier (DOI) 10.1007/s100520100787

THE EUROPEAN PHYSICAL JOURNAL C

Plasma production and thermalisation in a strong field

D.V. Vinnik[1], A.V. Prozorkevich[2], S.A. Smolyansky[2], V.D. Toneev[3], M.B. Hecht[4], C.D. Roberts[4], S.M. Schmidt[1]

[1] Institut für Theoretische Physik, Universität Tübingen, Auf der Morgenstelle 14, 72076 Tübingen, Germany
[2] Physics Department, Saratov State University, 410071 Saratov, Russian Federation
[3] Bogoliubov Laboratory of Theoretical Physics, Joint Institute for Nuclear Research, 141980 Dubna, Russian Federation
[4] Physics Division, Bldg 203, Argonne National Laboratory, Argonne, IL 60439-4843, USA

Received: 27 July 2001 /
Published online: 21 November 2001 –

Abstract. Aspects of the formation and equilibration of a quark–gluon plasma are explored using a quantum kinetic equation, which involves a non-Markovian, Abelian source term for quark and antiquark production and, for the collision term, a relaxation time approximation that defines a time-dependent quasi-equilibrium temperature and collective velocity. The strong Abelian field is determined via the simultaneous solution of Maxwell's equation. A particular feature of this approach is the appearance of plasma oscillations in all thermodynamic observables. Their presence can lead to a sharp increase in the time-integrated dilepton yield, although a rapid expansion of the plasma may eliminate this signal.

1 Introduction

The Relativistic Heavy-Ion Collider (RHIC) at Brookhaven National Laboratory and the Large Hadron Collider (LHC) at CERN are designed with the goal of producing an equilibrated phase of deconfined partonic matter: the quark–gluon plasma (QGP). Lattice-QCD simulations [1] and well-constrained phenomenological models [2] predict a second order phase transition at $T_c \simeq 150\,\mathrm{MeV}$; i.e., at energy densities $\gtrsim 1\,\mathrm{GeV/fm^3}$, in the equilibrium two light-flavour theory. For more than two flavours the characteristics of the transition are not as clear, but there is a transition. A number of phenomena have been proposed as signals for the existence of an equilibrated QGP [3] but the nonequilibrium stages in the plasma's development are poorly understood and it is a contemporary challenge to develop a description of the spacetime evolution of an ultra-relativistic heavy-ion collision (URHIC): from particle production in the collision, through equilibration and plasma formation, and on to hadronisation.

Two methods are commonly used to describe the production of partons in a collision: a perturbative pre-formed parton picture [4] and a nonperturbative flux-tube based picture [5]. They are complementary, and Monte Carlo event generators [6–8] and hydrodynamical models [9] have been developed to facilitate the analysis of data using either production model.

Herein we focus on the pre-equilibrium particle production stage in the evolution of a QGP and choose to employ a flux-tube model. In this model the two colliding nuclei are imagined to pass through one another and stretch a high energy-density flux tube between themselves as they separate. This flux tube, which describes the highly excited QCD vacuum, decays via a nonperturbative particle–antiparticle production process analogous to the Schwinger mechanism.

Particle production by the flux tube is described by a source term and in quantum field theory that source term is non-Markovian [10–15]; i.e., essentially nonlocal in time. This feature can be important when the fields are strong. (In the weak-field limit a time-local Schwinger-like source term is recovered.) Such a situation is plausible at RHIC and especially at LHC [2,15] where the anticipated initial energy densities are, respectively, $\varepsilon \sim 10$–$100\,\mathrm{GeV/fm^3}$ and $\varepsilon \gtrsim 1\,\mathrm{TeV/fm^3}$.

Another feature that is characteristic of the flux-tube production mechanism is the back-reaction phenomenon. This phrase simply describes the fact that once the particles are produced they are accelerated and thereby generate a field that interferes with the collisional field that produced them. Plasma oscillations are then almost inevitable [16], although they can rapidly be damped if the thermalising collisions between particles are frequent [14, 15,17–23].

An observable that may preserve information about non-Markovian effects and plasma oscillations in the pre-equilibrium particle production stage of an URHIC is the thermal dilepton spectrum, because leptons do not participate in the strong interactions that equilibrate the QGP [24]. To explore that possibility, we employ a quantum Vlasov equation with a non-Markovian source term to calculate the single particle distribution function that characterises particle production by the flux tube, $f(\boldsymbol{p}, t)$, and

use that to calculate the dilepton spectrum and its evolution from impact to equilibration.

Of course, equilibration can only be effected by dissipative processes, such as collisions, and herein we describe those effects via a relaxation time approximation (RTA). This is a coarse representation of the interactions between the partons produced in the collision but, even so, ensuring thermodynamic consistency is nontrivial. We introduce and describe one practical scheme for achieving that goal.

Our article is organised as follows. In Sect. 2 we present the quantum kinetic equation and review properties of the source term. The collision term is described in Sect. 3. This completes the specification of the model and so our results appear in Sect. 4. Section 5 presents some concluding remarks.

2 Distribution function

2.1 Kinetic equation and source term

We assume that in its wake an URHIC leaves a high energy-density electric field, which occupies a large (in fact, unbounded) spacetime volume. This excited domain decays via a Schwinger-like mechanism, producing an unequilibrated plasma of highly energetic quarks and antiquarks. That system evolves and equilibrates, forming a component of the QGP. Hadronisation only takes place at a later stage, when the temperature and density of the equilibrated system fall below some critical values, and herein we do not consider that process.

We represent the excited domain by a spatially homogeneous, time-dependent Abelian vector potential, $A_\mu(t)$, and work in the temporal gauge: $A_0 = 0$. The spatial part of the vector potential defines the $\hat{z}$-direction; i.e., $\boldsymbol{A}(t) = (0, 0, A(t))$, and generates an electric field $\boldsymbol{E}(t) = -\mathrm{d}\boldsymbol{A}(t)/\mathrm{d}t$. This provides the input for the quantum kinetic equations whose solution describes the evolution of the single parton distribution functions that characterise the produced partons:

$$\frac{\mathrm{d}}{\mathrm{d}t} f_\pm(\boldsymbol{p}, t) = S_\pm(\boldsymbol{p}, t) + C_\pm(\boldsymbol{p}, t), \tag{1}$$

where

$$\frac{\mathrm{d}}{\mathrm{d}t} := \frac{\partial}{\partial t} + eE(t)\frac{\partial}{\partial p_\parallel}, \tag{2}$$

e is the electric charge and $+/-$ denotes bosons/fermions; $f_\pm(\boldsymbol{p}, t)$ gives the ensemble fraction of particles with a given momentum, $\boldsymbol{p}$, at time t. The analogous equation for antiparticles, which is obtained via charge conjugation and must be solved simultaneously, yields $\bar{f}_\pm(\boldsymbol{p}, t)$, the single antiparticle distribution function. The feedback generated by the motion of the partons is incorporated by coupling Maxwell's equation to (1) and its analogue, as we discuss in Sect. 2.2. That also introduces a coupling between the equations for f, $\bar{f}$.

In (1), $C_\pm(\boldsymbol{p}, t)$ is the collision term, which also couples the equations for f and $\bar{f}$, and which we discuss in Sect. 3; and $S_\pm(\boldsymbol{p}, t)$ is the particle–antiparticle producing source term:

$$S_\pm(\boldsymbol{p}, t) = \frac{1}{2} W_\pm(\boldsymbol{p}, t, t) \int_{t_0}^{t} \mathrm{d}t' W_\pm(\boldsymbol{p}, t, t') \times [1 \pm 2 f_\pm(\boldsymbol{p}, t')] \cos\left[2 \int_{t'}^{t} \mathrm{d}\tau \omega(\boldsymbol{p}, t, \tau)\right]. \tag{3}$$

The effect of quantum statistics on the particle production rate is evident in the "$\pm 2 f_\pm$" in (3) (neglecting this term defines the low density limit) and in the different transition (or tunnelling) amplitudes

$$\mathcal{W}_\pm(\boldsymbol{p}, t, t') = eE(t') \frac{p(t, t')}{\omega^2(\boldsymbol{p}, t, t')} \left(\frac{\varepsilon_\perp}{p(t, t')}\right)^{g_\pm - 1}, \tag{4}$$

where $g_\pm = 2 s_\pm + 1$, with $s_+ = 0$, $s_- = 1/2$, the three-vector momentum $\boldsymbol{p} = (\boldsymbol{p}_\perp, p_\parallel)$, the transverse mass-squared $\varepsilon_\perp^2 = m^2 + p_\perp^2$, $\omega^2(\boldsymbol{p}, t, t') = \varepsilon_\perp^2 + p^2(t, t')$ and

$$p(t, t') = p_\parallel - e[A(t) - A(t')] = p_\parallel + e \int_{t'}^{t} \mathrm{d}\tau E(\tau). \tag{5}$$

(Equation (5), which describes the action of the field on the particles, is just a re-expression of the Lorentz force law: $\partial p(t, t')/\partial t = eE(t)$.) The source term is nonlocal in time and that can be important on short time-scales in strong fields: if the fields are strong enough the time duration of a tunnelling event and the time between successive events, which is set by the particles' Compton wavelengths, are similar, and the processes interfere, with observable consequences in the distribution function. In addition, strong fields enhance the differences between fermion and boson production. These features were highlighted in [10,13]. (For future reference we define the low density limit of the source term as $f_\pm(\boldsymbol{p}, t') \equiv 0$ on the r.h.s. of (3) and the Markov approximation as the replacement $f_\pm(\boldsymbol{p}, t') \to f_\pm(\boldsymbol{p}, t)$: $t' \to t$ here eliminates a nonlocality in time.)

With our initial setup we have a simple, algebraic symmetry between the particle and antiparticle distribution functions:

$$\bar{f}(\boldsymbol{p}, t) = f(-\boldsymbol{p}, t), \tag{6}$$

and hence it is only necessary to consider (1) explicitly. To simplify this kinetic equation we follow [14] and introduce two real auxiliary functions

$$u_\pm(\boldsymbol{p}, t) = \int_{t_0}^{t} \mathrm{d}t' W_\pm(\boldsymbol{p}, t, t')[1 \pm 2 f_\pm(\boldsymbol{p}, t')] \times \sin\left[2 \int_{t'}^{t} \mathrm{d}\tau \omega(\boldsymbol{p}, t, \tau)\right], \tag{7}$$

$$v_\pm(\boldsymbol{p}, t) = \int_{t_0}^{t} \mathrm{d}t' W_\pm(\boldsymbol{p}, t, t')[1 \pm 2 f_\pm(\boldsymbol{p}, t')] \times \cos\left[2 \int_{t'}^{t} \mathrm{d}\tau \omega(\boldsymbol{p}, t, \tau)\right], \tag{8}$$

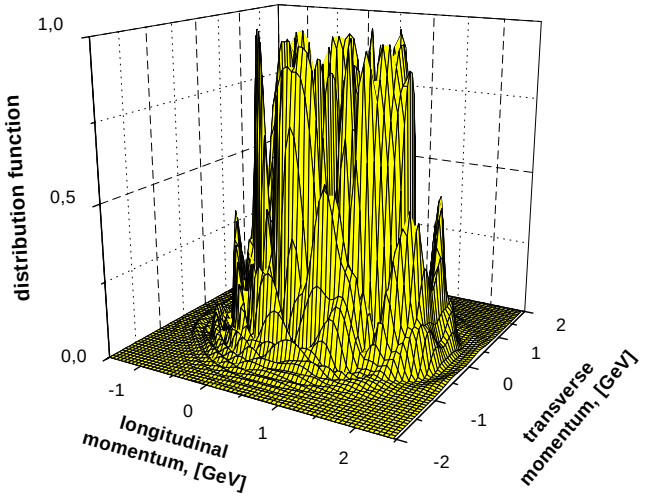

Fig. 1. Momentum dependence of the single parton distribution function: $f(\boldsymbol{p}, t = 10\,\mathrm{fm})$, obtained by solving (9)–(11) and (13)–(16), with the impulse profile in (12) ($A_0 = 1\,\mathrm{GeV}^2$, $1/b = 1\,\mathrm{GeV}$, and $mb = 1/5$; i.e., Set 4 in Table 1) and neglecting collisions. "transverse momentum" represents $|\boldsymbol{p}_\perp|$ and "longitudinal momentum" represents $p_\parallel$. The irregular structure makes it clear that this is not the distribution function of a system in equilibrium.

such that for $C_\pm(\boldsymbol{p}, t) = 0$: $u_\pm^2 + v_\pm^2 \mp (1 \pm 2f)^2 = \text{const.}$, with the initial conditions $f(t_0) = v(t_0) = u(t_0) = 0$. This permits us to rewrite (1) as a system of coupled, first order differential equations

$$\frac{\mathrm{d}}{\mathrm{d}t} f_\pm = \frac{1}{2} W_\pm(\boldsymbol{p}, t) v_\pm + C_\pm(\boldsymbol{p}, t), \tag{9}$$

$$\frac{\mathrm{d}}{\mathrm{d}t} u_\pm = 2\omega(\boldsymbol{p}) v_\pm \ , \tag{10}$$

$$\frac{\mathrm{d}}{\mathrm{d}t} v_\pm = W_\pm(\boldsymbol{p}, t)[1 \pm 2f_\pm] - 2\omega(\boldsymbol{p}) u_\pm, \tag{11}$$

where $W_\pm(\boldsymbol{p}, t)$ and $\omega(\boldsymbol{p})$ denote, respectively, $W_\pm(\boldsymbol{p}, t, t)$ and $\omega(\boldsymbol{p}, t, t)$. While this complex is qualitatively identical to (1), it is simpler to treat numerically.

The kinetic equation describes pair creation for both bosons and fermions. In the following we identify the fermionic degrees of freedom with the quarks and antiquarks produced in an URHIC and restrict ourselves solely to the fermionic case, henceforth suppressing the $\pm$ subscript.

2.2 Maxwell's equation and internal currents

The kinetic equation depends nonlinearly on the time-dependent electric field. The URHIC provides the impetus for this field: it provides an external field, which we model via

$$E_{\mathrm{ex}}(t) = -A_0 \mathrm{sech}^2(t/b). \tag{12}$$

This profile "switches on" at $t \sim -2b$ and off at $t \sim 2b$, and attains its maximum magnitude of A_0 at $t = 0$.

Table 1. Parameter sets used to specify our model of an URHIC, (12). They yield equilibrium values of thermodynamic quantities (three rightmost columns) that are consistent with those expected in a QGP, with Sets 3, 4 approximating RHIC-like conditions. We use $mb = 1/5$, a strong coupling: $e = 1$, $\tau_\mathrm{c} = 1$, and consider 3 quark flavours, which explains the factor of $N_p = 18 = 2_{\mathrm{spin}} 3_{\mathrm{flavour}} 3_{\mathrm{colour}}$ that appears frequently. (Using the low density limit to the source term or the Markov approximation alters the calculated values of ε, T, n by $\leq 5\%$ for Set 1. However, these approximations introduce an error of as much as 35% for Set. 4.)

	A_0 [GeV^2]	b [fm]	ε [GeV/fm^3]	T [GeV]	n [fm^{-3}]
Set 1	0.25	0.2	1.0	0.20	1.4
Set 2	0.40	0.2	2.5	0.26	3.0
Set 3	0.75	0.2	12	0.38	10
Set 4	1.0	0.2	24	0.44	17

The external field, E_{ex}, polarises the vacuum, generating a polarisation current that depends on the dielectric properties of the medium, which are encoded in the source term, and promotes the spontaneous production of particle–antiparticle pairs, which it then accelerates, generating a conduction current that depends on the particle distribution function. A consequence of the URHIC then is the appearance of a two component internal current and an attendant internal electric field:

$$-\dot{E}_{\mathrm{in}}(t) = j_{\mathrm{in}} = j_{\mathrm{cond}}(t) + j_{\mathrm{pol}}(t), \tag{13}$$

where the fully renormalised currents are [14]

$$j_{\mathrm{cond}}(t) = 2N_p e \int \frac{\mathrm{d}^3 p}{(2\pi)^3} \frac{p_\parallel}{\omega(\boldsymbol{p})} f(\boldsymbol{p}, t), \tag{14}$$

$$j_{\mathrm{pol}}(t) = N_p e \int \frac{\mathrm{d}^3 p}{(2\pi)^3} \frac{\varepsilon_\perp}{\omega(\boldsymbol{p})} \left[v(\boldsymbol{p}, t) - \frac{e\dot{E}(t)\varepsilon_\perp}{4\omega^4(\boldsymbol{p})} \right], \tag{15}$$

with $N_p = 18$, as described in Table 1.

In the absence of collisions, (9)–(11) and (13)–(15), with

$$E(t) = E_{\mathrm{ex}}(t) + E_{\mathrm{in}}(t), \tag{16}$$

form a closed system of coupled equations whose solution provides the time-dependent electric field and single parton distribution function. We can use this system to illustrate some of the effects we have mentioned. In Fig. 1 we depict the momentum dependence of the distribution function. The irregular structure is produced by interference effects in the non-Markovian source term, which arise because the tunnelling time is of the same magnitude as the Compton wavelength of the produced particles, and by the feedback mechanism. This structure is averaged out in the ideal Markov limit [10] and makes it very clear that this is *not* the distribution function of a system in equilibrium. Figure 2 depicts the time evolution of the calculated distribution function and the feedback that characterises

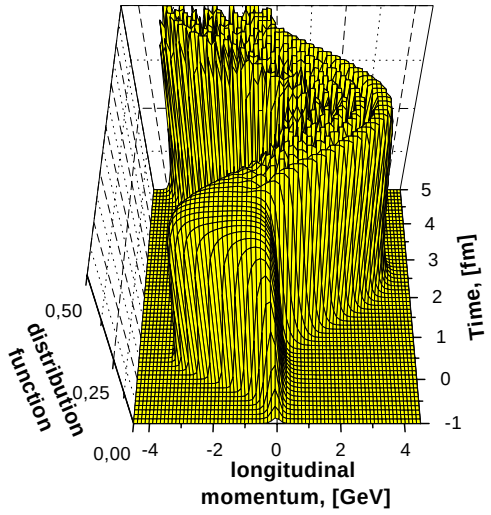

Fig. 2. Time evolution of the single parton distribution function: $f(p_\perp = 0, p_\parallel, t)$ in the low density limit. (Model parameters are as in Fig. 1.) The regular (plasma) oscillation is driven by the back-reaction phenomenon.

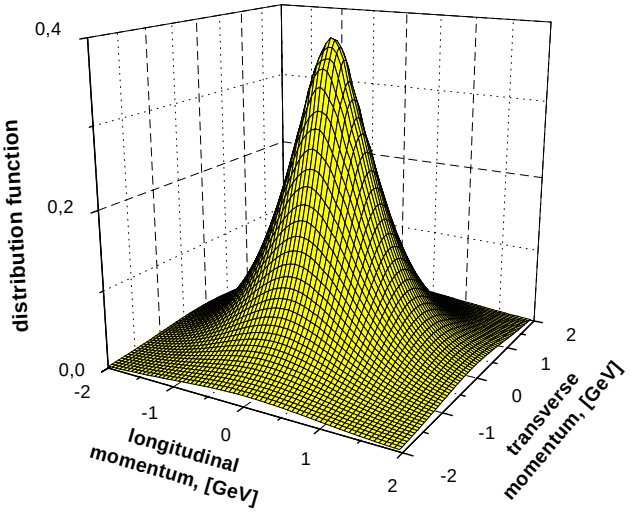

Fig. 3. $f(\boldsymbol{p}, t = 10\,\mathrm{fm})$ obtained with the inclusion of parton–parton collisions, as described in Sect. 3. Collisions promote equilibration of the system, which is evident in the now smooth distribution function; cf. Fig. 1. (Model parameters are as in Fig. 1).

the behaviour of the internal currents is manifest in the obvious, regular plasma oscillation. For comparison, in Fig. 3 we depict the distribution function obtained after the inclusion of dissipative effects, to be discussed in Sect. 3.

3 Equilibrating collisions

Once the particles are produced they are accelerated by the electric field and, as we saw in Sect. 2.2, if $eE \sim \varepsilon_\perp^2$, then large amplitude, high frequency plasma oscillations appear. This collective effect, which is a hallmark of the flux-tube approach, may have observable consequences in experiments aimed at producing an equilibrated QGP. Whether that is the case or not can only be determined once the effect of parton–parton collisions is incorporated.

The general nature of the dissipative collision term is known: it too is non-Markovian and can produce particles [25]. However, its complexity mitigates against its use in semi-quantitative, exploratory studies and hence herein we employ a simple RTA [14,15,18–23].

In this approach the detailed description of parton–parton scattering is replaced by a continuous viscosity term, which involves a time-dependent parameter that is identified with the collision period. In addition we suppose that the thermodynamic laws are valid at each time t, and this assumption of local-equilibrium provides us with an internally consistent definition and calculation of time-dependent thermodynamic variables, such as temperature and energy density. Of course, accepting a physical interpretation of these quantities only makes sense once the violent effects of the URHIC have subsided and the quantities are evolving slowly with t.

The collision term in the kinetic equation for $f(\boldsymbol{p}, t)$ must describe particle–particle (pp) and particle–antiparticle (pa) collisions and reflect the symmetries of our initial conditions. Hence we employ

$$C(\boldsymbol{p}, t; T, u^\nu) = \frac{1}{\tau_{\mathrm{pp}}(t)} \left[f_{\mathrm{eq}}(\boldsymbol{p}, t; T(t), u^\nu(t)) - f(\boldsymbol{p}, t) \right] + \frac{1}{\tau_{\mathrm{pa}}(t)} \left[f_{\mathrm{eq}}(-\boldsymbol{p}, t; T(t), u^\nu(t)) - f(\boldsymbol{p}, t) \right], \tag{17}$$

where $\tau_{\mathrm{pp}}(t) = \tau_{\mathrm{pa}}(t) = \tau(t)$ is the time-dependent relaxation time, and

$$f_{\mathrm{eq}}\left(\boldsymbol{p}, T, u^\nu\right) = \left[\exp\left(\frac{p_\nu u^\nu(t)}{T(t)} \right) + 1 \right]^{-1} \tag{18}$$

is the quasi-equilibrium distribution function, with p_ν the quarks' four-momentum. The other quantities in (17) are

$$u^\nu(t) = (1, 0, 0, u(t))[1 - u(t)^2]^{-(1/2)}, \tag{19}$$

the hydrodynamical four-velocity and $T(t)$, the local-equilibrium temperature, both of which we define below.

Our RTA encodes all the complicated effects of parton–parton collisions in a single time-dependent quantity, the relaxation time $\tau(t)$. It is a measure of the time between successive collisions and as such can be expressed as [23]

$$\tau(t) = \tau_{\mathrm{c}} \frac{\lambda(t)}{\bar{v}(t)}, \tag{20}$$

where $\lambda(t) = 1/[n(t)]^{1/3}$ is the mean interparticle separation, since

$$n(t) = N_p \int \frac{\mathrm{d}^3 p}{(2\pi)^3} f(\boldsymbol{p}, t) \tag{21}$$

is the mean particle number density, and

$$\bar{v}(t) = |\boldsymbol{p}|_f(t)/\varepsilon_f(t) \tag{22}$$

is an average speed. (See (23) and (27).) The only parameter in our implementation of the relaxation time approximation is then τ_c, the dimensionless constant of proportionality.

Returning to (17), we define the local temperature by requiring that at each time t the mean particle energy density in the plasma is identical to that in an equilibrated plasma at a temperature $T(t)$; i.e.,

$$\varepsilon_f(t) = N_p \int \frac{\mathrm{d}^3p}{(2\pi)^3}\omega(\boldsymbol{p})\,[f(\boldsymbol{p},t) - z_f(\boldsymbol{p},t)] \quad (23)$$

$$= N_p \int \frac{\mathrm{d}^3p}{(2\pi)^3}\omega(\boldsymbol{p}) f_{\mathrm{eq}}(\boldsymbol{p},t). \quad (24)$$

Similarly, $u(t)$ in (19) is defined via the requirement

$$\boldsymbol{p}_f(t) = N_p \int \frac{\mathrm{d}^3p}{(2\pi)^3}\boldsymbol{p}\,[f(\boldsymbol{p},t) - z_f(\boldsymbol{p},t)] \quad (25)$$

$$= N_p \int \frac{\mathrm{d}^3p}{(2\pi)^3}\boldsymbol{p} f_{\mathrm{eq}}(\boldsymbol{p},t); \quad (26)$$

i.e., that the mean particle three-momentum is the same as that of an equilibrated plasma characterised by an hydrodynamical particle velocity $u(t)$. The average magnitude of the momentum is

$$|\boldsymbol{p}|_f(t) = N_p \int \frac{\mathrm{d}^3p}{(2\pi)^3}|\boldsymbol{p}|\,[f(\boldsymbol{p},t) - z_f(\boldsymbol{p},t)]\,. \quad (27)$$

The new element in these equations,

$$z_f(\boldsymbol{p},t) = \left(\frac{e\mathcal{E}_\perp}{4\omega^3(\boldsymbol{p})}\right)^2 \times \left[E^2(t) - \frac{2}{\tau_c}\mathrm{e}^{-2t/\tau_c}\int_{t_0}^{t}\mathrm{d}t' E^2(t')\mathrm{e}^{2t'/\tau_c}\right], \quad (28)$$

is a regularising counterterm, determined via the same procedure [14] that yields the renormalised currents in Sect. 2.2, which ensures that the integrals involving the calculated distribution function are finite. This counterterm itself exhibits "memory effects;" i.e., it is sensitive to the time-history of the electric field.

We judge that using a time-dependent relaxation time is an improvement over previous work that used $\tau(t) =$ const.; e.g., [14,15], because it is manageable and better models the conditions produced by an URHIC. Clearly, just after the impact the parton number density is small and hence the time between successive collisions is large. Over time, however, the density of produced partons increases, leading to a reduction in the interval between collisions. These features are crudely reflected by the evolution of the relaxation time described in (20).

The final form of our collision term is thus obtained from the combination of (17) and (20); i.e.,

$$C(\boldsymbol{p},t) = \frac{\bar{v}(t)}{\lambda(t)}\left(\frac{f_{\mathrm{eq}}(\boldsymbol{p},T(t),u(t)) - f(\boldsymbol{p},t)}{\tau_c} + \frac{f_{\mathrm{eq}}(-\boldsymbol{p},T(t),u(t)) - f(\boldsymbol{p},t)}{\tau_c}\right). \quad (29)$$

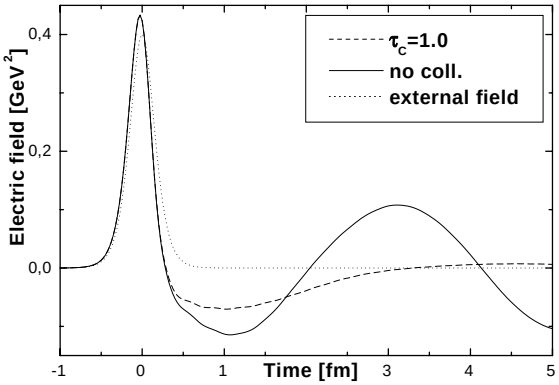

Fig. 4. Time evolution of the total electric field. The effects of feedback are evident in the oscillatory behaviour of $E(t)$. The viscous collision term damps these oscillations in a characteristic time $\tau_c/m \sim 1$fm. The external impulse electric field is also depicted. (Parameters: Set 2, Table 1).

It provides additional nonlocal feedback in the solution for $f(\boldsymbol{p},t)$. We emphasise again that our RTA is based on the assumption of local-equilibrium, which is valid for $|t| \gg b$, where b is the time duration of the URHIC. For $|t| \lesssim b$, however, it is of questionable validity and may lead to model-dependent artefacts, the misinterpretation of which one must guard against.

4 Numerical results

4.1 Thermodynamic parameters

Our results are obtained via the simultaneous solution of (9)–(11), (13)–(15), (24)–(28), using the collision term in (29), which we accomplish using a fourth order Runge–Kutta procedure. The solution, $f(\boldsymbol{p},t)$, fully describes the plasma's evolution, from its creation to equilibration. In addition we obtain the time-dependent vector potential, electric field and currents, and also the quasi-equilibrium temperature and collective velocity.

To explore the solution's properties we have employed a range of parameter sets, which are listed in Table 1, and in Figs. 4–9 we demonstrate the effect of collisions by comparing the solution obtained using $\tau_c = 1.0$ with that obtained in the collisionless limit $\tau_c \to \infty$. (As is evident in the figures, the plasma period satisfies $m\tau_{\mathrm{pl}} \approx 2.5 \sim \tau_c$. For $\tau_c \ll m\tau_{\mathrm{pl}}$ plasma oscillations are not observable [14]; i.e., the system is overdamped.)

In Fig. 4 we see that the URHIC generates a strong electric field, which produces particles that sustain the field for a time that depends on the collision frequency: a large value of $\nu_c = 1/\tau_c$ means a short-lived electric field and rapid equilibration.

Figure 5 depicts the time evolution of the energy density, (23). It is negative on a small domain around $t = 0$ because of the large vacuum polarisation induced by the strong external field. This instability is quickly corrected by rapid particle creation; a correlation that is apparent in a comparison of Fig. 5 with Fig. 6, which portrays the particle number density, (21). The density reaches a higher

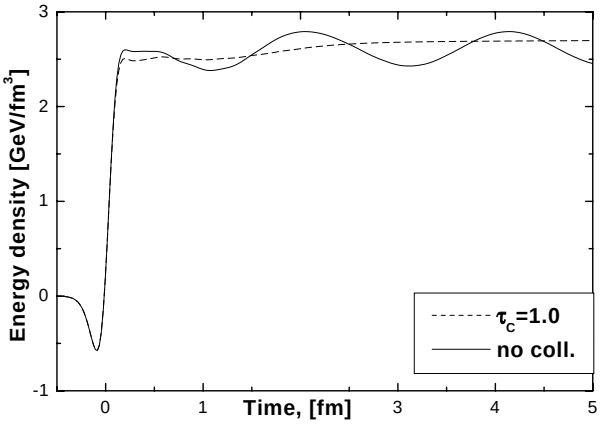

Fig. 5. Time evolution of the calculated energy density, (23). It is negative in the neighbourhood of $t = 0$ because of the large vacuum polarisation produced by the strong external field (the URHIC). This feature is quickly compensated by particle production in the aftermath of the impact. Collisions subsequently yield an equilibrated QGP. (Parameters: Set 2, Table 1).

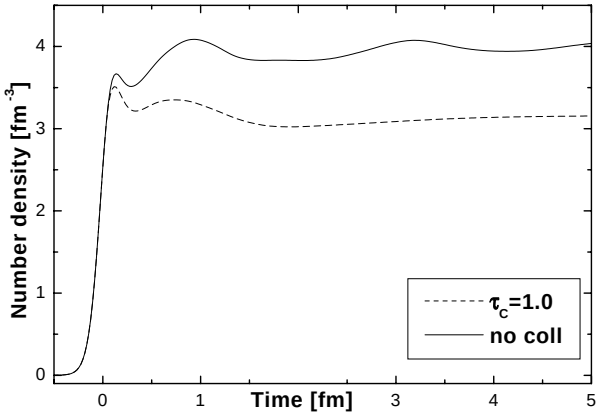

Fig. 6. Time evolution of the particle number density, (21). The equilibrium value: 3.0 fm^{-3}, is that listed in Table 1. (Parameters: Set 2, Table 1).

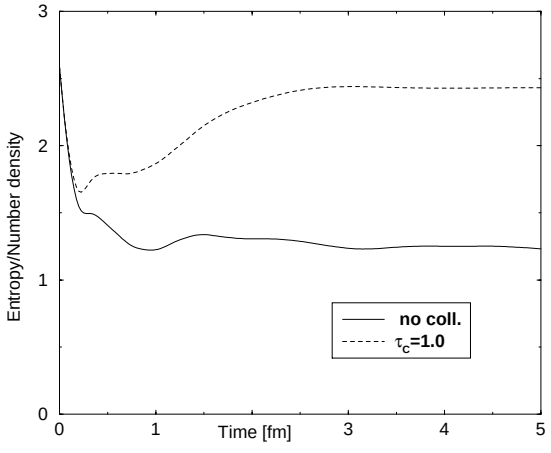

Fig. 7. Time evolution of the entropy/particle, (30), with and without collisions. It is intuitively obvious why the entropy is larger when particle–particle collisions are incorporated: in equilibrating the system, collisions increase the degree of disorder. (Parameters: Set 2, Table 1).

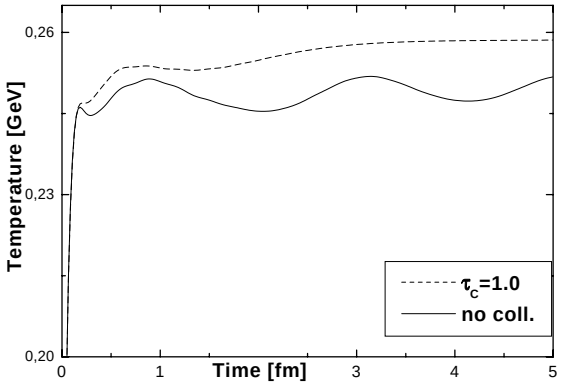

Fig. 8. Time evolution of the quasi-equilibrium temperature. The equilibrium value reached here, 0.26 GeV, is greater than the anticipated critical temperature for QGP formation. (Parameters: Set 2, Table 1).

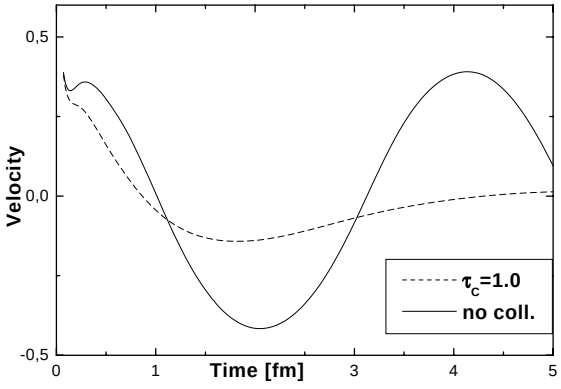

Fig. 9. Time evolution of the collective velocity, $u(t)$. Its behaviour clearly signals the collective plasma oscillation that is characteristic of the flux-tube production mechanism. The plasma oscillation is damped by collisions. (Parameters: Set 2, Table 1).

value in the absence of collisions because the field–current feedback allows unhindered, repeated bursts of particle-pair creation. The Pauli principle does not significantly retard the process because, while the particles are preferentially produced with small momenta, the field rapidly accelerates them. As Table 1 shows, the number density increases with increasing A_0; i.e., with increasing impulse field strength.

In Fig. 7 we plot the behaviour of the entropy/particle, where the entropy density is

$$s(t) = -N_p \int \frac{\mathrm{d}^3 p}{(2\pi)^3} \{ f(\boldsymbol{p},t) \ln f(\boldsymbol{p},t) - [1 - f(\boldsymbol{p},t)] \ln[1 - f(\boldsymbol{p},t)] \} . \quad (30)$$

The calculated quasi-equilibrium temperature is depicted in Fig. 8. After rising quickly, it settles into a slow evolution once the external field, (12), has subsided. This marks the beginning of the domain on which the concept of local equilibrium is valid.

The local velocity is plotted in Fig. 9. It shows, as one would intuitively expect, that the produced particles are

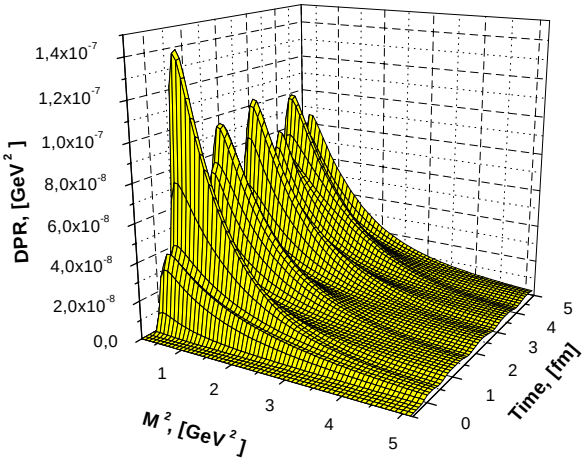

Fig. 10. Time evolution of the dilepton production rate. The plasma oscillation is evident in this collisionless case, as is the feature that the dileptons are preferentially produced at low M^2. (Parameters: Set 4, Table 1).

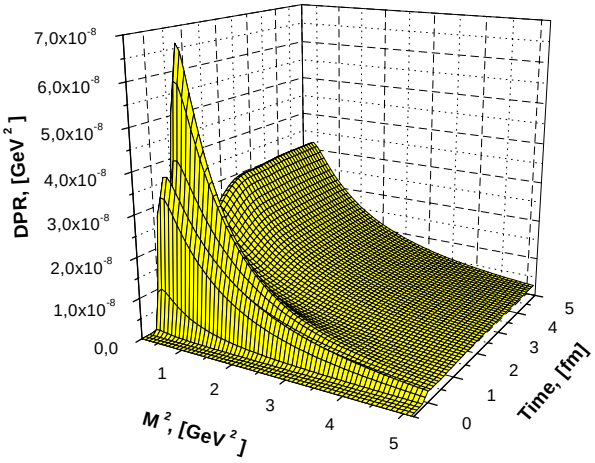

Fig. 11. Time evolution of the dilepton production rate. Frequent collisions rapidly damp the plasma oscillation, forcing the production rate to settle at a constant value. (Parameters: Set 4, Table 1).

accelerated, reaching their maximum velocity when the electric field vanishes (cf. Fig. 4), then decelerated as the field reverses direction. They stop, and then reverse direction and are accelerated by the reversed field to a new maximum velocity. The repetition of this pattern is the collective plasma oscillation, which is clearest in this figure. Of course, in equilibrating the system, collisions act to destroy the pattern.

4.2 Dilepton production

The plasma oscillation is evident in the electric field and in each of the thermodynamic variables, but none of these quantities are directly measurable. Is there any way that this characteristic signature of the flux-tube production mechanism can be observed?

The thermal dilepton production rate may provide a means. Dileptons produced in the URHIC do not interact strongly and hence those produced soon after the impact carry and transmit information about the pre-equilibrium stage of the plasma. The dilepton production rate from our (quasi-) equilibrium three quark system can be estimated using [24,26]

$$\begin{aligned}\frac{\mathrm{d}N}{\mathrm{d}t\mathrm{d}^3x\mathrm{d}M^2} &= \frac{\alpha^2}{3\pi^3}(1-4m_l^2/M^2)^{1/2}\left(1+2\frac{m^2+m_l^2}{M^2}+4\frac{m^2m_l^2}{M^4}\right)\\ &\times\int_m^\infty \mathrm{d}\epsilon_1\mathrm{d}\epsilon_2 f(\epsilon_1)f(\epsilon_2)\theta(M^2-M_-^2)\\ &\times\theta(M_+^2-M^2),\end{aligned} \tag{31}$$

where $\alpha = 1/137$; m_l is the lepton mass, m the quark mass and we use $m_l = m$; M^2 is the invariant mass of the produced dilepton pair;

$$M_\pm^2 = 2m^2 + 2\epsilon_1\epsilon_2 \pm 2|\boldsymbol{p}_1||\boldsymbol{p}_2|, \tag{32}$$

and the time dependence of the distribution functions is implicit.

We obtain the distribution functions, $f(\epsilon_{1,2})$ in (31), as described in Sect. 4.1, using the RHIC-like parameter Set 4 in Table 1. Knowing them, the calculation of the dilepton production rate is straightforward. In Fig. 10 we display that rate as a function of (M^2, t). The plasma oscillation is evident in the time evolution, with more dilepton pairs being produced when the electric field is strongest and the parton production rate peaks, and no pairs being produced when the electric field vanishes. The effect of collisions is to drive the system to equilibrium where the thermal dilepton production rate becomes constant, as shown in Fig. 11.

Clearly, the plasma oscillations generate a signal. However, the time evolution of the dilepton production rate is a difficult quantity to measure. An easier quantity is the time-integrated rate:

$$\rho_{l^+l^-}(t) := \frac{\mathrm{d}N}{\mathrm{d}^3x\mathrm{d}M^2} = \int_0^t \mathrm{d}t' \frac{\mathrm{d}N}{\mathrm{d}t'\mathrm{d}^3x\mathrm{d}M^2}. \tag{33}$$

Does a signal survive in this observable?

In Fig. 12 we plot $\rho_{l^+l^-}(t)$ obtained in the absence of collisions, which must be compared with the function in Fig. 13 that was obtained with the inclusion of collisions. Our simple model yields rates that are comparable with other estimates; e.g., [27], and the comparison of the figures shows that plasma oscillations generate an enhancement in the number of dileptons, $\rho_{l^+l^-}(t)$, which is as large as a factor of 2 at $t = 5\,\mathrm{fm}$, given the Set 4 initial conditions in Table 1. (Note that collisions eliminate the plasma oscillation, so Fig. 13 can be thought of as the oscillation-free scenario.)

A further illustration of the effect is provided in Fig. 14. The equilibrium energy per particle, ε/n, grows with the violence of the collision, i.e., with the value of A_0, as do the amplitude and frequency of the plasma oscillations. This effect is responsible for the sharp increase in the dilepton

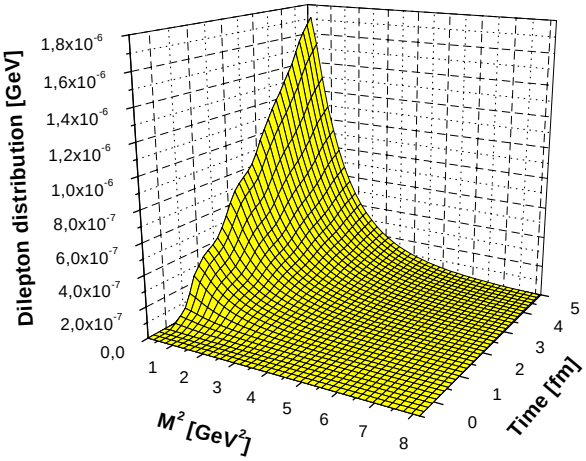

Fig. 12. Time integrated dilepton production rate, (33), calculated without collisions and hence in the presence of a persistent plasma oscillation. (Parameters: Set 4, Table 1).

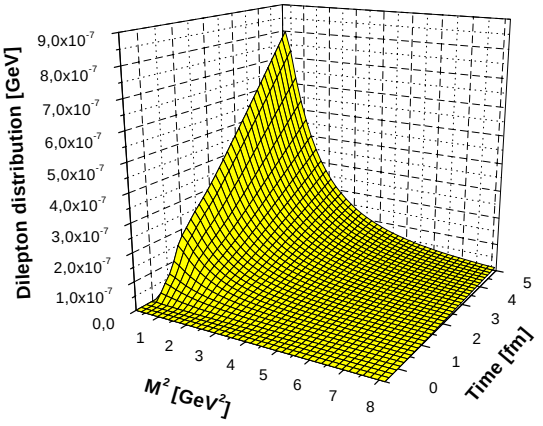

Fig. 13. Time integrated dilepton production rate, (33), calculated under the influence of frequent collisions that rapidly equilibrate the plasma. (Parameters: Set 4, Table 1).

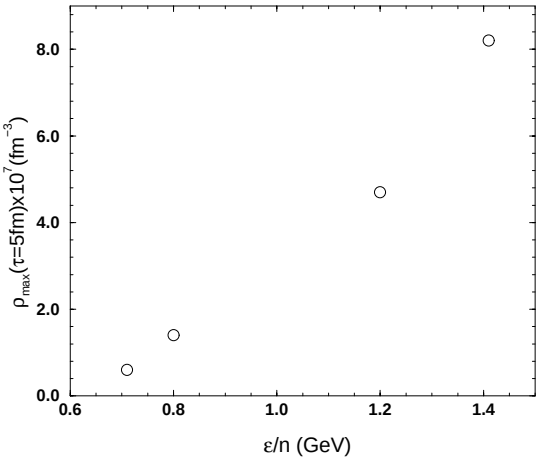

Fig. 14. $\rho_{l^+l^-}(t = 5\,\mathrm{fm})$ at the low invariant mass, M^2, for which it takes its maximum value, as a function of the equilibrium energy/particle attained in the collisions described by the parameter sets in Table 1. The sharp increase in $\rho_{l^+l^-}$ occurs after the plasma oscillation overpowers the viscous collision term.

yield, evident in Fig. 14, for the most energetic collision in Table 1. At lower values of ε/n the effect of plasma oscillations is suppressed by collisions, but for the Set 4 initial conditions the magnitude and frequency of the plasma oscillation are large enough to make their action evident in spite of the damping, at least in our idealised treatment. (A rapid expansion of the plasma will alter the initial conditions required for plasma oscillations to have observable consequences. It may even eliminate all possibility of an observable signal.)

5 Epilogue

We have used a quantum kinetic equation coupled with Maxwell's equation to explore the formation and equilibration of a strong field plasma. Using a simple impulse model for the URHIC, which produces RHIC-like conditions, we find that the non-Markovian aspects of the source term do not generate observable effects. However, the field–current feedback, which is characteristic of the production of strongly coupled charges by a strong field, manifests itself in the appearance of plasma oscillations in the thermodynamic observables. The oscillations are also evident in the production rate of thermal dileptons and, while the time evolution of this rate may not be measurable, the plasma oscillations act to significantly enhance the time-integrated rate. The effect is marked by a sharp increase in the dilepton yield when the energy per particle becomes large enough to generate a high frequency and large amplitude plasma oscillation, which initially overwhelms the effect of collisions.

While the magnitudes of the quantities we calculate are phenomenologically reasonable, the primary results of our study are qualitative and many improvements are possible. Our relaxation time approximation to the collision term is an intuitive and practical tool but a more realistic connection with the actual collision process would provide a systematic and well-constrained quantitative improvement. A simpler step is the introduction of a strongly momentum-dependent dressed-parton mass, which is an essential feature of QCD [28]. That can have a significant impact on the evolution of the plasma, promoting plasma oscillations [29], and also on its subsequent hadronisation [30]. Perhaps the most significant defect of our study is the use of an Abelian model for the colour fields and progress with a non-Abelian transport equation would be a marked improvement [19].

Acknowledgements. We thank R. Alkofer, V. Morozov and P.C. Tandy for helpful discussions. This work was supported by the Deutsche Forschungsgemeinschaft under project nos. SCHM 1342/3-1 and 436 RUS 17/102/00-17/54/01, the US Department of Energy, Nuclear Physics Division, under contract no. W-31-109-ENG-38, the US National Science Foundation under grant no. INT-9603385 and partly by the Russian Federation's State Committee for Higher Education under grant

no. N 97-0-6.1-4. This research benefited from the resources of the National Energy Research Scientific Computing Center.

References

1. E. Laermann, Fiz. Élem. Chastits At. Yadra **30**, 720 (1999) [Phys. Part. Nucl. **30**, 304 (1999)]
2. C.D. Roberts, S.M. Schmidt, Prog. Part. Nucl. Phys. **45**, S1 (2000)
3. S.A. Bass, M. Gyulassy, H. Stöcker, W. Greiner, J. Phys. G G **25**, R1 (1999); S. Scherer et al., Prog. Part. Nucl. Phys. **42**, 279 (1999); U. Heinz, M. Jacob, Evidence for a new state of matter: An assessment of the results from the CERN lead beam programme, nucl-th/0002042
4. L.V. Gribov, M.G. Ryskin, Phys. Rept. **189**, 29 (1990)
5. B. Andersson, G. Gustafson, G. Ingelman, T. Sjöstrand, Phys. Rept. **97**, 33 (1983)
6. X. Wang, M. Gyulassy, Phys. Rev. D **44**, 3501 (1991)
7. K. Geiger, Phys. Rept. **258**, 237 (1995)
8. B. Andersson, G. Gustafson, B. Nilsson-Almquist, Nucl. Phys. B **281**, 289 (1987); K. Werner, Phys. Rept. **232**, 87 (1993)
9. M. Gyulassy, T. Matsui, Phys. Rev. D **29**, 419 (1984); K. Kajantie, R. Raitio, P.V. Ruuskanen, Nucl. Phys. B **222**, 152 (1983); G. Baym, B.L. Friman, J.P. Blaizot, M. Soyeur, W. Czyż, Nucl. Phys. A **407**, 541 (1983)
10. Y. Kluger, E. Mottola, J.M. Eisenberg, Phys. Rev. D **58**, 125015 (1998)
11. S.M Schmidt D. Blaschke, G. Röpke, S.A. Smolyansky, A.V. Prozorkevich, V.D. Toneev, Int. J. Mod. Phys. E **7**, 709 (1998)
12. S.A. Smolyansky, G. Röpke, S.M. Schmidt, D. Blaschke, V.D. Toneev, A.V. Prozorkevich, hep-ph/9712377; S.M. Schmidt, A.V. Prozorkevich, S.A. Smolyansky, Creation of boson and fermion pairs in strong fields, Proceedings V. Workshop on Nonequilibrium Physics at Short Time Scales, April 27–30, 1998, hep-ph/9809233
13. S.M. Schmidt, D. Blaschke, G. Röpke, A.V. Prozorkevich, S.A. Smolyansky, V.D. Toneev, Phys. Rev. D **59**, 094005 (1999)
14. J.C.R. Bloch, V.A. Mizerny, A.V. Prozorkevich, C.D. Roberts, S.M. Schmidt, S.A. Smolyansky, D.V. Vinnik, Phys. Rev. D **60**, 116011 (1999)
15. J.C.R Bloch, C.D. Roberts, S.M. Schmidt, Phys. Rev. D **61**, 117502 (2000)
16. Y. Kluger, J.M. Eisenberg, B. Svetitsky, F. Cooper, E. Mottola, Phys. Rev. Lett. **67**, 2427 (1991); F. Cooper, J.M. Eisenberg, Y. Kluger, E. Mottola, B. Svetitsky, Phys. Rev. D **48**, 190 (1993)
17. K. Kajantie, T. Matsui, Phys. Lett. B **164**, 373 (1985); G. Gatoff, A.K. Kerman, T. Matsui, Phys. Rev. D **36**, 114 (1987)
18. B. Banerjee, R.S. Bahlerao, V. Ravishankar, Phys. Lett. B **224**, 16 (1989)
19. G.C. Nayak, V. Ravishankar, Phys. Rev. D **55**, 6877 (1997); ibid. C **58**, 356 (1998)
20. A. Bialas, W. Czyż, A. Dyrek, W. Florkowski, Nucl. Phys. B **296**, 611 (1988)
21. S. Mrówczński, Phys. Rev. D **39**, 1940 (1989)
22. G. Baym, Phys. Lett. B **138**, 18 (1984)
23. G.C. Nayak, A. Dumitru, L. McLerran, W. Greiner, Equilibration of the gluon-minijet plasma at RHIC and LHC, hep-ph/0001202
24. L.D. McLerran, T. Toimela, Phys. Rev. D **31**, 545 (1985); D. Boyanovsky, H.J. de Vega, R. Holman, S. Prem Kumar, Phys. Rev. D **56**, 5233 (1997); A. Drees, Understanding Deconfinement in QCD, edited by D. Blaschke, F. Karsch, C.D. Roberts (World Scientific, Singapore 2000) pp. 285–290
25. T.S. Biro, C. Greiner, Phys. Rev. Lett. **79**, 3138 (1997); W.M. Alberico, A. Lavagno, P. Quarati, Eur. Phys. J. C **12**, 499 (2000); O.V. Utyuzh, G. Wilk, Z. Wlodarczyk, J. Phys. G **26**, L39 (2000)
26. C.Y. Wong, Introduction to high-energy heavy-ion collisions (World Scientific, Singapore 1994)
27. D. Dutta, K. Kumar, A.K. Mohanty, R.K. Choudhury, Phys. Rev. C **60**, 014905 (1999)
28. C.D. Roberts, Continuum strong QCD: Confinement and dynamical chiral symmetry breaking, nucl-th/0007054; P. Maris, Continuum QCD and light mesons, nucl-th/0009064
29. A.V. Prozorkevitch, D.V. Vinnik, M.B. Hecht, C.D. Roberts, S.M. Schmidt, Pair Creation and Plasma Oscillations, in the Proceedings of Quark Matter in Astro- and Particlephysics, Rostock, Germany, November 27–29, 2000, nucl-th/0012039
30. P. Božek, Y.B. He, J. Hüfner, Phys. Rev. C **57**, 3263 (1998)